sustainability

MDPI

Article

Evaluating Mineral Matter Dynamics within the Peatland as Reflected in Water Composition

Valentina Pezdir *, Luka Serianz and Mateja Gosar

Geological Survey of Slovenia, Dimičeva ulica 14, 1000 Ljubljana, Slovenia; luka.serianz@geo-zs.si (L.S.); mateja.gosar@geo-zs.si (M.G.)

* Correspondence: valentina.pezdir@geo-zs.si

Abstract: Peatland hydrology plays an important role in preserving or changing the record in any consideration of past atmospheric deposition records in peat bogs. The Šijec bog, located on the Pokljuka plateau in Slovenia, is one of the largest ombrotrophic peatlands. We sampled the surface pools, pore water, drainage from the peatland, and karst streams not connected to the peatland. Additionally, we sampled the precipitation, as ombrotrophic peatlands receive mineral matter solely from the atmosphere. The results of the evaluation of the chemical and isotopic composition indicated different origins of dissolved mineral matter in different water types. The components originating from the bedrock and surrounding soils (Ca, Mg, Al, Si, Sr) predominated in the streams. The chemical composition of the peatland drainage water revealed the significant removal of major components from the peatland, particularly elements like Al, Fe, and REE, and metals that are readily dissolved in an acidic environment or mobile in their reduced state. Despite their solubility, concentrations of metals (As, Cr, Cu, Fe, Ni, Pb, Ti) and REE in surface pools remained higher than in the drainage due to incomplete elimination from the peatland. The composition of pore water reflects variations among the W and E parts of the peatland, indicating a heterogenous hydrological structure with different dynamics, such as an additional source of water at approximately 90 cm depth in the NW part. The chemical composition and isotope signature (^{18}O and ^{2}H) of pore water additionally indicated a heterogeneous recharge with residence times of less than a year. The overall analysis indicated a predominantly ombrotrophic type and a small part in the NW area of the peatland as a minerotrophic type of peat.

Keywords: peatland; hydrogeochemistry; isotopes

Citation: Pezdir, V.; Serianz, L.; Gosar, M. Evaluating Mineral Matter Dynamics within the Peatland as Reflected in Water Composition. *Sustainability* **2024**, *16*, 4857. https://doi.org/10.3390/su16114857

Academic Editor: Yong Xiao

Received: 25 March 2024
Revised: 30 May 2024
Accepted: 3 June 2024
Published: 6 June 2024

1. Introduction

Alpine peatlands occur in alpine, sub-alpine, and mountain regions around the world and are frequently found in the Alps, as well as in the Andes, on the Tibetan plateau, in the Australian Alps, and in other regions of the world [1]. The effects of global warming can be particularly harmful to ecosystems like peatlands [2,3]. Peatlands are highly sensitive environments that are dependent on their hydrology, as it influences oxygen and gas diffusion rates, redox status, and the availability of nutrients and cycling, as well as species composition and diversity [4]. Therefore, peatland degradation due to natural processes, such as climate change and the development of gullies, and anthropogenic influences, such as ditch excavation and grazing, all negatively affect the ecosystems and ecological functions of peatlands [5–7]. Although the degradation of peatlands essentially refers to the transformation of organic into inorganic mineral soils (decomposition), caused by biogeochemical processes and microbial activities [8,9], these processes and activities are closely related to changes in the peatland hydrology [7].

Ombrotrophic peatlands with precipitation as their only source of water [10,11] are highly acidic, with a pH of less than 4, whereas minerotrophic peatlands with additional groundwater sources are less acidic [4]. The chemistry of peat water reflects the input water

and the chemical transformations within the peat system, including the decay processes [12]. The movement of water within peat is greatly impeded in cases of dense peat with a fine peat matrix and small pore spaces. In some ombrotrophic peatlands, the horizontal movement of water can predominate over vertical water movement due to variations in the hydraulic conductivity [12].

Due to the acidic and organic-matter-rich environments of peatlands [12] and their redox conditions [13], mineral matter deposited on the peatland is partially or completely dissolved. The elements may then be retained in the peatland environment due to vegetation, physical retention, or binding in complex compounds. Some major and trace elements may be removed from the peatland (e.g., Zn and Ni), while others are retained or move within the peat profile (e.g., Pb and Cu) [14].

Karst areas supply a large source of inorganic carbon to peatlands and are important in the dissolved inorganic carbon (DIC) cycle [15,16]. The pH of peatland pore water increases with the increased inflow of water that is rich from carbonate dissolution, especially with present groundwater or lateral inflow [16].

The loss of carbon during the decomposition of organic matter enriches the bound components in peat [17]. Dissolved organic matter (DOM) derived from the decomposition of plant remains in peatlands can also act as a major carrier of trace elements [18,19] in the peatland outflow. However, DOM is not presumed to be the main control for the mobilization of elements with a high affinity for binding to DOM [20]. Instead, it is suggested that mobilization is mainly influenced by decomposition and transport based on hydrology [20]. The discharge of peat water occurs mainly in the upper peat layers (acrotelm) in the areas characterized by fluctuations in the water table [21].

Stable isotopes of water ($\delta^{18}O$ and $\delta^{2}H$) can be used to trace the hydrologic cycle in peat-dominated catchments (e.g., [22,23]). The $\delta^{18}O$ value of precipitation is influenced by the effects of temperature, the relative humidity, precipitation events, the air mass history, the amount, the circulation, the altitude and latitude effects, the form of precipitation (snow, rainfall), and the source region of the moisture [24–26]. Stable isotopes of hydrogen and oxygen are also useful tools for determining the residence time [27], to indicate the potential water inputs to the system, and to determine the mixing of waters of different origin within the system [28,29]. Determining groundwater storage and its change in peatland is essential for revealing the complex mechanisms that cause the degradation of peatlands [7].

Ombrotrophic bogs are distinctive ecohydrological systems that contribute towards the creation of various habitats. The major driving force behind these habitats is the hydrological cycle, which is reflected in the condition and composition of the raised bog vegetation [30,31]. The predominance of Sphagnum moss is an important indication of ombrotrophication, as Sphagnum has the ability to raise the acidity and anoxicity of peatlands [32]. Additionally, the isolation of the peatland from alkaline water increases the abundance of Sphagnum mosses and stabilizes the hydrology of the peatland [33,34].

In Slovenia, there is a small number of relatively small bogs on the Pokljuka, Pohorje, and Jelovica plateaus [35], as a specific morphological feature formed by glaciers. In the Slovenian Alpine region, the total peatland area is estimated at 4 km^2 [36]. One of the most prevalent bogs in the wider Alpine region is the Šijec bog. The Šijec bog is formed on the carbonaceous bedrock of the Pokljuka carbonate massive. Glaciers, as well as the karstic nature of carbonate rocks, helped to create favorable conditions for the formation of pots, which were slowly deposited by some clayed sediments and persisted during the last glacial maximum [37]. The characterization of the chemical and isotopic composition of the surface waters in the area of the Šijec bog provides valuable insight into the possible processes and influences on the peatland hydrology. Understanding these processes is crucial for any further analysis of peat chemical compositions and understanding the peatland dynamics. In this study, we examined the relationship between precipitation, surface waters, and pore water on the peatland and its surroundings, with a specific focus on the unanswered research questions related to the formation of Alpine peat and the hydrological cycle in karstic environments.

In this study, we aim to describe changes in the water chemistry in peatland environments that occur naturally. These changes can be amplified when peatlands are subjected to sudden changes, due to anthropogenic influence or long-term changes in environments due to climate change. Understanding the dynamics of the dissolved mineral matter within peatlands and their surroundings presents important information on water quality and the potential risk for the surrounding environment, especially in areas where peatlands present a larger surface area.

In the case of the Šijec bog, this study presents insight into the water chemistry and properties, which in combination with studies of peatland formation, atmospheric deposition, and the geochemical properties of peat organic and mineral matter, will provide information on the preservation of mineral matter in peat. This will help with the evaluation of peat potential as a tracer of past atmospheric deposition and present the potential risk of mineral matter release due to changes in the peatland environments.

2. Study Area

The Pokljuka is an extensive karst plateau in NE Slovenia with an elevation of approximately 1200 to 1500 m. It has a relatively flat topography, bordering on valleys in the S, SW, and E of the area. It borders on a high mountain range in the NE. The Pokljuka plateau area is part of Triglav National Park. The surface water in a karst environment is only found in karst springs and peatlands [38,39]. Glacial deposits after the retreat of the glacier are isolated in small lakes, from which the peatlands formed [37]. Among the largest peatland on the Pokljuka plateau is Šijec bog. It covers approximately 15 hectares and is located 1194 m above sea level. Due to its altitude, the Šijec bog, as well as the Pokljuka plateau, is characterized by a typical Alpine climate. The snow coverage is long-term, 4–6 months annually, and the vegetation period is short, at only 3–4 months.

The Šijec bog has a relatively flat topography with elevated edges (Figure 1), the highest of them is along the southern border, where it reaches an elevation of 1198 m. The bog's lowest point lies in its northwestern part, where a larger depression is apparent, at 1191 m above sea level. Although the Šijec bog covers a relatively small area, it has a complex structure. It consists of four peat basins, ranging in depth from 6 to 9 m, separated with ridges overlying the glacial deposits from previous ice ages [37]. The shallower basins are located in the E part of the peatland, where a slight dome structure is observed (Figure 1), indicating the potential formation of ombrotrophic peat. The largest and deepest basin is located in the NW part and represents the wettest area, with many Sphagnum pools [37,40], and coincides with the lowest elevation in the area of the peatland (Figure 1). The elevated areas and edges of the peatland are drier and covered with mountain pine bushes. The flat areas are largely covered with Sphagnum moss and grasses. The peatland is surrounded by a dense spruce forest [41].

According to previous geological [42,43] and geomorphological mapping [44] of the Pokljuka plateau, glacial deposits (moraines) of different ages and Triassic limestones are present on the surface in the vicinity of the Šijec bog. In the wider area of Šijec bog, there are reef limestones with corals, massive limestones [45], and limestones with chert [46,47], which can also be found in small windows throughout the glacial deposits [45]. The base of the peatlands is represented by lacustrine sediments [45]. The peat, clay, and sandy clay deposits of lacustrine origin belong to the Pleistocene and Holocene periods [43,48].

Due to the predominant karstic terrain, which is occasionally covered by moraine sediments, the infiltration rate is high, which leads to relatively short surface water flows. The surface water is present in the form of small surface pools on the peatland surface and small streams SW and NW of the Šijec bog area. The latter includes two streams with different orientations, and both represent the surface drainage for the bog. The streams in the S-N general direction originate from the edge of the peatland and have small tributaries. An E-W direction stream has a karst spring at the foot of the hill. Both streams are short (150–200 m) and flow into a sinkhole, marked in Figure 1. In the SW area, the peatland gradually changes into a wetland, where a stream flowing in a NE-SW direction forms.

Downstream, the stream joins with tributaries that are connected to the peatlands in the vicinity of the Šijec bog. The length of the stream is dependent on the weather conditions, with a dry channel present only in the dry seasons. The wettest conditions are present in the spring after the melting of the snow, when the streams and two drainage systems are easily visible (NW and SW area of the peatland; Figure 1). As these streams flow in a karst environment, the surrounding geology greatly influences the chemical composition of the water.

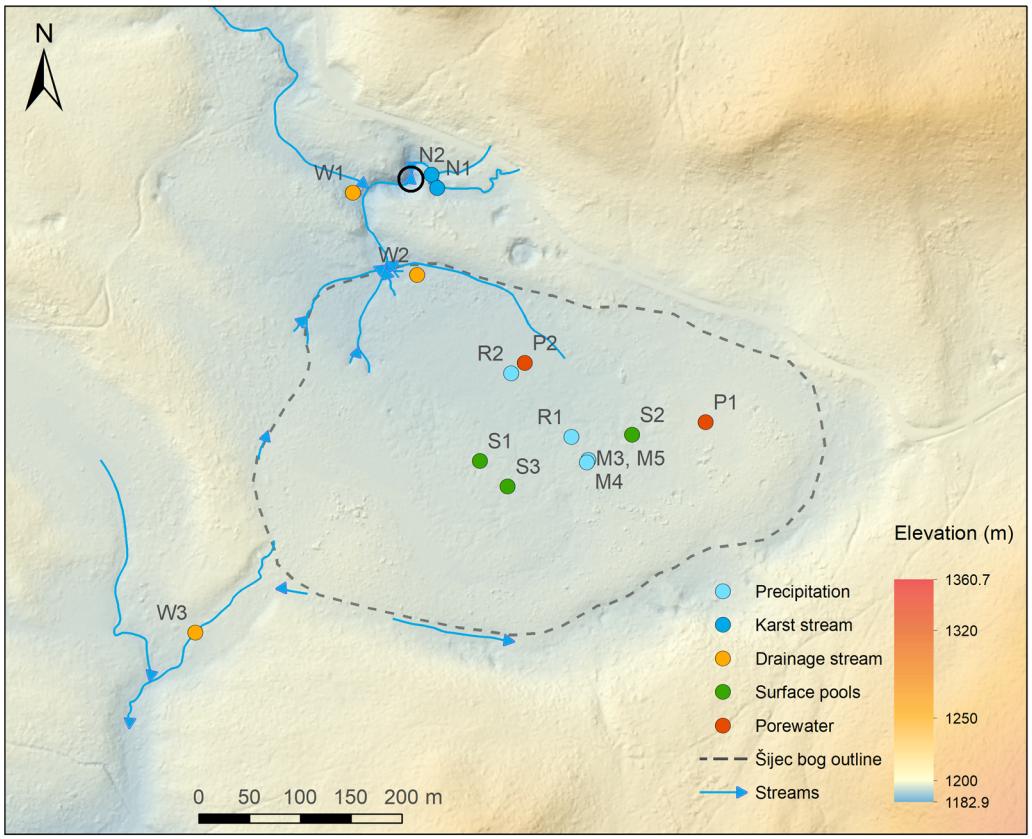

Figure 1. Location of the Pokljuka plateau in Slovenia and locations of the sampling points on the Šijec bog and surroundings with labelled water types. The elevation is exaggerated in the low values to emphasize the topography of Šijec bog. The black circle marks the location of the sinkhole.

3. Materials and Methods

The surface waters in the area of the Šijec bog were divided into three categories: (1) the karst streams (which had no contact with the peatland); (2) the streams that included drainage from the peatland; and (3) the pools on the peatland surface (Figure 1). Two sampling points were determined along the karst stream (N1 and N2). Regarding the streams that featured drainage from the peatland, we determined sampling points next to the peatland (W2) and further downstream along the same stream (W1) in the NW area. Another point (W3) was determined in the SW area. The sampling points at locations W1 and W3 were determined upstream from any confluence points with the stream tributaries. For the sampling water on the surface of the peatland, we chose three separate pools that were present throughout the year. All the samples were filtered using Minisart 0.45 µm syringe filters (Sartorius, Göttingen, Germany) during the sampling and stored at 8 °C prior to the chemical analysis.

The pore water was collected at two locations in the peatland (Figure 1). The E area of the Šijec bog (P1) had a higher elevation (1198 m), with numerous drier hummocks present on the surface. In contrast, the NW area (P2) was topographically lowest with an elevation of 1192 m and consisted of many sphagnum pools, with the water table near the surface

throughout the year. The sampling point P1 was located in the shallowest peat basin (peat thickness 6 m) and point P2 was located in the deepest basin, with the peat thickness exceeding 9 m [37]. In each location, the pore water was sampled at three depths—30, 60, and 90 cm—using Macrorhizon samplers (Eijkelkamp, Giesbeek, The Netherlands), the field equivalent of the Rhizon soil moisture samplers [49]. The sampler was inserted in the peat, and by producing a vacuum, the sample accumulated in the 10-cm-long porous tube.

In order to observe the composition of the input water to the peatland, we collected precipitation. We collected rainwater (two samples in 2020 and two samples in 2021, as well as four snowmelt samples in 2020 and three samples in 2021). The samples were first filtered using isopore membrane polycarbonate filters (<0.6 µm) (Merck KGaA, Darmstadt, Germany) to separate the solid particles [50] and later filtered through 0.45 µm Minisart syringe filters prior to the chemical analyses.

The physico-chemical parameters (pH, electroconductivity—EC, oxidation reduction potential—ORP, and dissolved oxygen in water—RDO) were measured at all selected locations using the multiparameter meter Thermo Scientific Orion Star A329 (Thermo Scientific, Waltham, MA, USA). The samples consisted of 50 mL of water for the chemical analysis and 50 mL for the isotope analysis. The measurements and the collection of the samples were performed in different seasons and conditions throughout the year to observe the seasonal changes.

Analysis of the stable isotopes of $\delta^{18}O$ and $\delta^{2}H$ was performed using a Picarro L2130-I laser isotopic analyzer, by Picarro, Inc., Santa Clara, CA, USA based on wavelength scanned cavity ring-down spectroscopy (WS-CRDS) with a precision of (1d) 0.03/0.1% for $\delta^{18}O/\delta^{2}H$ [51,52]. Isotope analysis was evaluated by IAEA Water Stable Isotope Intercomparison [53].

The correction equation was based on the measurement of the primary standards USGS 46, 47, and 48 with known values [54–56], together with in-house standards calibrated periodically against primary USGS standards. The typical drift over 24 h without recalibration was 0.08‰ and 0.3‰ for $\delta^{18}O$ and $\delta^{2}H$, respectively [51]. The stable isotopic compositions of hydrogen and oxygen were normally reported as delta (δ) values as parts per thousand (‰), relative to a standard VSMOW [57]:

$$\delta^{Y}Z(\%) = (R_X/R_S - 1) \times 100, \quad (1)$$

where YZ is ^{18}O or ^{2}H, R denotes the ratio of the heavy (less abundant) to light (more abundant) isotope ($^{2}H/^{1}H$, $^{18}O/^{16}O$), and RX and RS are the ratios in the sample (x) and standard (s). The analysis is described in more detail in Koren et al. [58].

An isotopic analysis was not performed for samples P1-30 and P2-90 due to the low amount of the samples and for sample N2 due to an error, possibly related to the higher pH value (8.2).

The stable isotopic composition was compared with the Global Meteoric Water Line (GMWL), defined as $\delta^{2}H = 8\delta^{18}O + 10$ (‰) [59], the Eastern Mediterranean Meteoric Water Line (EMMWL), defined as $\delta^{2}H = 8\delta^{18}O + 22$ [60], and the Local Meteoric Water Lines Kredarica, defined as $\delta^{2}H = 8.4\delta^{18}O + 19$, and for Zgornja Radovna, defined as $\delta^{2}H = 8\delta^{18}O + 11$ [61].

The isotopic analyses of $\delta^{18}O$ enabled a rough estimation of the groundwater mean residence time (MRT). The estimate was based on a periodic regression analysis to fit the seasonal sine curve to the $\delta^{18}O$ time series [62]. Seasonal trends in the $\delta^{18}O$ value were modelled using Origin Pro [63] to fit the seasonal sine wave curves to the variations in the annual $\delta^{18}O$ value of the precipitation and groundwater [27]. Further, the mean residence times (T) of the water leaving the system were estimated using an exponential model using the following equation [27]:

$$T = c^{-1}\left[(A_{z2}/A_{z1})^{-2} - 1\right]^{0.5} \quad (2)$$

where A_{z1} is the amplitude of precipitation $\delta^{18}O$, A_{z2} is the amplitude of the stream water, and c is the radial frequency of the annual fluctuations (0.017214 rad d-1). In this study, $\delta^{18}O$ data from the Kredarica meteorological station for the period 15/7/2018 to 15/6/2020 [39,64] were taken into account in order to calculate the amplitude of precipitation.

The water samples were sent to Activation Laboratories Ltd., where they were first acidified and analyzed using inductively coupled plasma (ICP) and mass spectrometry (MS) with a lower detection limit. The analysis was performed for 63 elements: Ag, Al, As, B, Ba, Be, Bi, Br, Ca, Cd, Ce, Co, Cr, Cs, Cu, Dy, Er, Eu, Fe, Ga, Gd, Ge, Hf, Hg, Ho, I, In, K, La, Li, Lu, Mg, Mn, Mo, Na, Nb, Nd, Ni, Pb, Pr, Rb, Re, Sb, Sc, Se, Si, Sm, Sn, Sr, Ta, Tb, Te, Th, Ti, Tl, Tm, U, V, W, Y, Yb, Zn, and Zr.

Quality control was achieved using the analysis of 17 duplicates (eight performed in the laboratory and nine taken in the field) and standards (IV-STOCK-1643 [65]). We eliminated the elements Mn, Na, Pb, Se, Ti, and Zn, as their analytical errors exceeded 30%. Additionally, we eliminated those elements where more than 30% of the values were below the detection limit (LOD). As only a few values for the remaining elements were below the detection limit, we replaced those with ½ the value of the limit of detection [66]. In the statistical analysis, we therefore used Al, As, Ba, Ca, Ce, Co, Cr, Cu, Fe, K, La, Mg, Mo, Nd, Ni, Rb, Sb, Si, Sr, V, Y, and Zr. From the precipitation samples, we also eliminated Ni and Y as most values were below the limit of detection.

The statistical analysis was performed using the TIBCO Statistica software v.13 [67]. The graphical presentation was performed using Grapher software v.19 by GoldenSoftware.

4. Results and Discussion

4.1. Precipitation

Precipitation is slightly acidic (pH from 5.5. to 6.5), with low electrical conductivity (EC) values from 3 to 7.5 µS/cm. The lower values were observed in snow, while the higher values were characteristic of rainwater, due to the possible dissolution of solid particles in the samplers during the sampling period. The variations between samples occurred between the snow samples, as some (M1-2, M2-2, M5) contained traces of a dust event. Additionally, pH and EC could be affected by the dissolution of carbonates in rainwater. The physico-chemical parameters measured in the rainwater and snowmelt samples are described in detail in Pezdir et al. [50].

Rainwater has very low concentrations of elements, similar to or lower than the typical concentrations of dissolved ions for continental rainwater [68]. Snowmelt water also exhibits very low values. Many elements (Al, Ba, Ca, Cu, Fe, K, Mg, Si, and Sr) show greatly increased concentrations after dust events. This was especially well observed in samples from February and March 2021, when a dust event occurred between both samplings [69] (e.g., from 10.4 µg/L to 46.3 µg/L for the Al concentration). Similarly, an increase was also visible in samples from March 2020 (e.g., from 33 µg/L to 66.5 µg/L for the K concentration). The said increase was best observed for elements related to silicates and carbonates, which corresponded with findings in Pezdir et al. [50], as these elements were also the most abundant in the dry atmospheric deposition particles. No dust events occurred during the rainwater sampling. The concentrations in rainwater from both sampling locations increased in 2021 compared with 2020. As the samples were taken under similar weather conditions and were exposed on the peatlands for the same time period, these changes in concentration could reflect the influence of COVID-19. Regarding the biomonitoring of air pollution, Zupančič and Bozau [70] studied the levels of potentially toxic elements (PTE) in sphagnum mosses in different locations, including the Šijec bog on the Pokljuka plateau. They concluded that the observed elements had higher levels in 2019 compared with 2020 due to the COVID-19 lockdown.

The stable isotope composition of precipitation (Table 1) fell on the Global Meteoric Water Line (GMWL), with its trendline equation defined as $\delta^{2}H = 8\delta^{18}O + 9.2$ (‰) (Figure 2). In 2020, precipitation was deposited as both rain and snow during the rainwater sampling, and due to the low temperatures (average 2.6 °C), evaporation was slow, which resulted in

low contents of the ^{18}O stable isotope. In contrast, the temperatures were higher during the rainwater sampling in 2021, with an average of 11.8 °C. Higher evaporation resulted in enrichment with the heavier ^{18}O isotope. The stable isotope composition of snow (Table 1) was comparable with the average winter values, which fell on the GMWL [58,71], as well as most local meteoric water lines (LMWL) established in Slovenia [61,72].

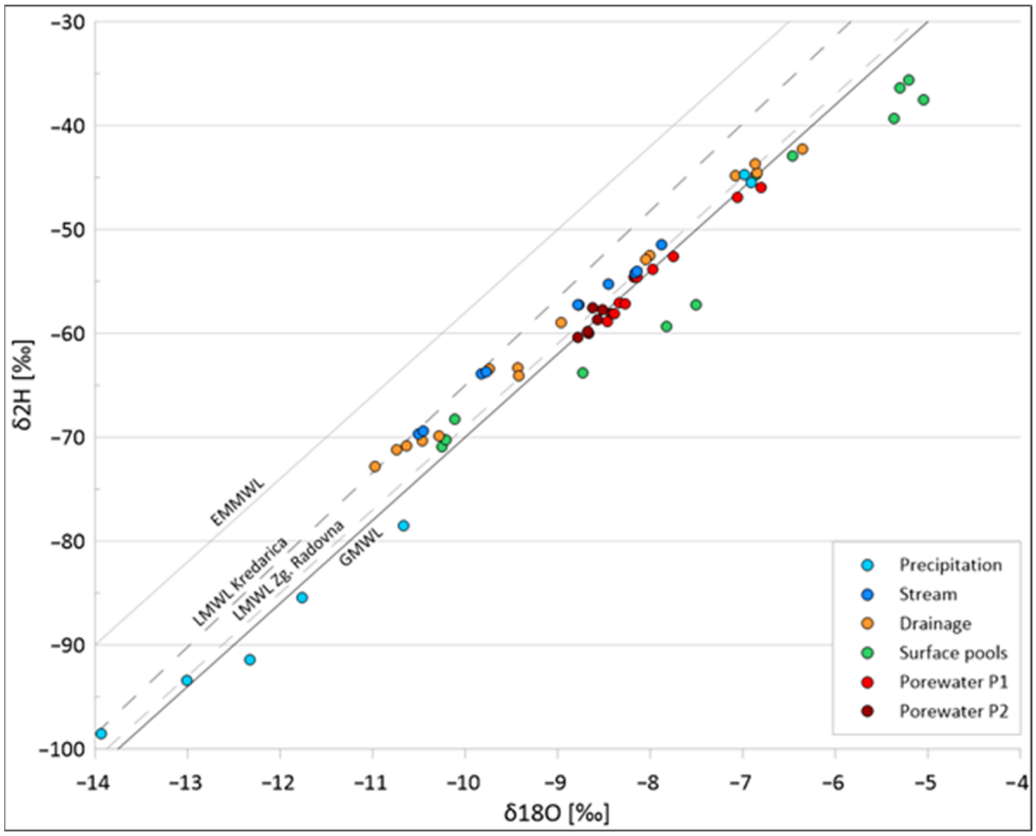

Figure 2. Results of the stable isotope analysis, with Global Meteoric Water Line (GMWL), East Mediterranean Meteoric Water Line (EMMWL), and Local Meteoric Water Lines (LMWL).

Table 1. Results of the isotope analysis.

Sample	Isotope	Nov-20	Mar-21	Aug-21	Sep-21	Oct-21	May-22	Jun-22	Nov-22	Dec-22
N1	^{18}O	−8.77	−9.82	−8.45	−8.17		−10.51		−9.15	−9.42
	^{2}H	−57.27	−63.91	−55.23	−54.24		−69.72		−59.4	−60.78
N2	^{18}O	−8.78	−9.77	−7.88	−8.14		−10.45			−9.42
	^{2}H	−57.29	−63.71	−51.47	−54.04		−69.42			−61.21
W1	^{18}O	−9.43	−10.74	−6.84	−7.08		−10.46		−8.48	−9.99
	^{2}H	−63.35	−71.21	−44.56	−44.83		−70.35		−54.6	−65.65
W2	^{18}O	−9.42	−10.97	−6.35	−6.86		−10.28		−8.34	−10.15
	^{2}H	−64.07	−72.83	−42.25	−43.65		−69.88		−53.6	−66.85
W3	^{18}O	−8.96	−9.74	−8.01	−8.05		−10.63		−8.71	−9.45
	^{2}H	−59.01	−63.43	−52.51	−52.88		−70.83		−55.69	−61.07
S1	^{18}O	−10.25		−5.3	−5.36		−7.5		−8.15	−10.89
	^{2}H	−70.96		−36.33	−39.29		−57.29		−53.51	−72.83

Table 1. *Cont.*

Sample	Isotope	Nov-20	Mar-21	Aug-21	Sep-21	Oct-21	May-22	Jun-22	Nov-22	Dec-22
S2	^{18}O	−10.11		−6.85	−6.46		−8.73		−8.58	−9.39
	^{2}H	−68.25		−44.69	−42.94		−63.79		−55.19	−62.27
S3	^{18}O	−10.21		−5.21	−5.05		−7.82		−8.11	−10.33
	^{2}H	−70.3		−35.59	−37.54		−59.38		−52.81	−68.57
P1-30	^{18}O			−7.06	−6.80	−7.75				
	^{2}H			−46.89	−45.99	−52.64				
P1-60	^{18}O			−7.97	−8.14	−8.39		−8.76		
	^{2}H			−53.84	−54.61	−58.08		−58.12		
P1-90	^{18}O			−8.33	−8.27	−8.46		−8.65		
	^{2}H			−57.1	−57.15	−58.88		−57		
P2-30	^{18}O			−8.18	−8.42	−8.78		−9.34		
	^{2}H			−54.64	−58.07	−60.41		−62.64		
P2-60	^{18}O			−8.52	−8.62	−8.67		−9.03		
	^{2}H			−57.71	−57.56	−60.01		−59.89		
P2-90	^{18}O			−8.57		−8.67		−9.1		
	^{2}H			−58.71		−59.83		−60.45		
R1	^{18}O	−13.01								
	^{2}H	−93.4								
R2	^{18}O	−13.93								
	^{2}H	−98.54								
R3	^{18}O				−6.91					
	^{2}H				−45.49					
R4	^{18}O				−6.98					
	^{2}H				−44.70					
M3	^{18}O		−10.66							
	^{2}H		−78.49							
M4	^{18}O		−12.32							
	^{2}H		−91.44							
M5	^{18}O		−11.76							
	^{2}H		−85.40							

4.2. Surface Water and Pore Water

4.2.1. Isotopic Composition and Estimated Residence Times

The karst streams showed seasonal variations (Figure 3), with the lowest values when the surface of the peatland was frozen or covered with snow (late autumn, winter, and spring) and the highest in the summer. The melting of the ice released the lighter ^{16}O and therefore yielded lower ^{18}O values. In the summer, higher temperatures caused the preferential evaporation of the lighter oxygen isotope (^{16}O), causing the water to be enriched with ^{18}O.

The streams with the drainage and surface pools exhibited more expressed seasonal variations (Figure 3). The surface pools are shallow water bodies and therefore experienced higher temperatures in the summer (>20 °C) and were frozen in winter. The heavier oxygen isotope was enriched in the summer and early autumn, when the evaporation was highest, and depleted in the winter (sampling in November 2020 and December 2022). Low ^{18}O values in winter could be affected by the melting of the snow in water. The isotopic composition indicated differences between the sampling points of the surface pools, as the seasonal variations were not as defined in the E part (sampling point S2), as they were in

the central part of the peatland (sampling points S1 and S3) (Figure 3). Seasonal variations could be affected by variations in the size and shallow depth of the pools. Although all the pools were relatively small in size, they could vary from 1 to 5 m in diameter and 5 to 40 cm in depth.

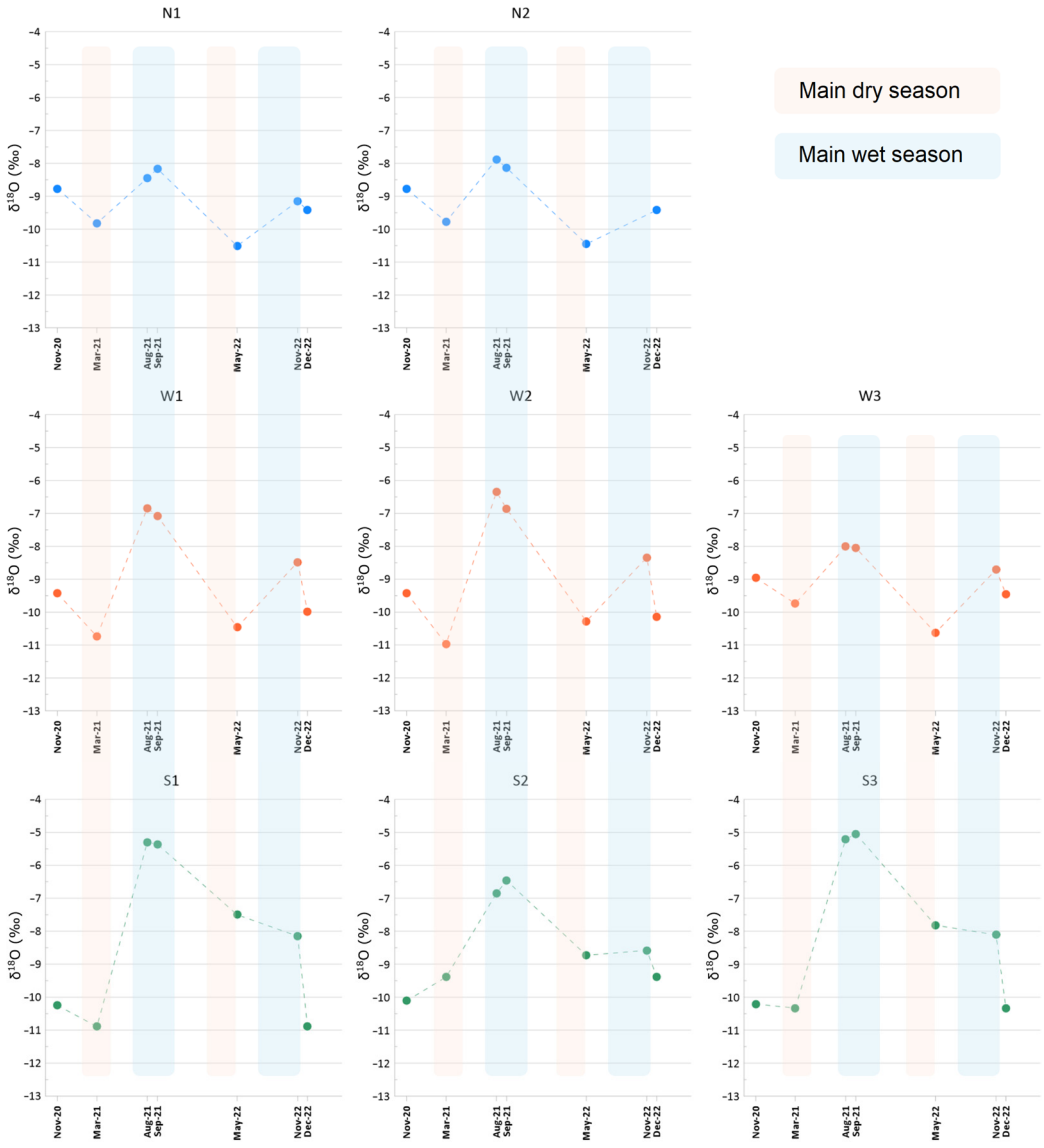

Figure 3. Seasonal variations in the ^{18}O isotope for the different water types. As the measurements are not sequential, the line represents approximate variations. Main wet (late summer and autumn) and dry seasons (winter) are marked.

The value of ^{18}O in the surface pools was especially higher in the summer (from −7 to −5‰) than it was in the streams (from −9 to −7‰). This could be due to the local temperatures, which were higher on the peatland surface in the spring, compared with the forest and the narrow stream gorge. This was also confirmed with the water temperatures, as the streams had average values from 4 °C to 10 °C, while the average water temperature in the surface pools was 18 °C. In the colder time of the year, the differences were smaller or even lower in the surface pools (−11‰ in the pools and −10‰ in the streams).

There were not enough pore water samples to establish seasonal variations, though the comparison with other water types showed a relatively stable composition.

Based on the ^{18}O variations and amplitudes, it was estimated from Equation (2) that the residence time of all the water samples was up to approximately 6 months. Hence, the lowest amplitude and the longest residence times of approximately 5 to 6 months could be observed for the stream water, which represented the recharging water outside of the peatland area. In the surface pools, the estimated residence times were low and could only be calculated for S2, while at the other two water samples, the amplitude values were higher (3.51 ± 0.72 and 3.50 ± 0.77 for S1 and S3, respectively) than the precipitation amplitude at Kredarica (3.33; Table 2). This was to be expected due to the presence of the prevailing precipitation-based water in the surface pools (Table 2).

Table 2. Sampling sites, amplitudes, and residence times.

Sampling Point	Object Type	Discharge (L/s)	Amplitude	R^2	T (Years) Based on Zgornja Radovna
Kredarica	Rain gauge	/	3.33	0.43	/
N1	Stream	0.3 *	0.99 ± 0.28	0.81	0.51
N2	Stream	0.2 *	1.13 ± 0.39	0.81	0.44
S1	Surface pools	/	3.51 ± 0.72	0.90	/
S2	Surface pools	/	2.09 ± 0.68	0.77	0.20
S3	Surface pools	/	3.50 ± 0.77	0.88	/
W-1	Drainage	5 **	2.29 ± 0.33	0.94	0.17
W-2	Drainage	1 **	2.64 ± 0.32	0.94	0.12
W-3	Drainage	<0.01 *	1.13 ± 0.88	0.95	0.44

* Estimation on June 14, 2023. ** Measurements with OTT MF Pro Portable Flow Meter on June 14, 2023.

Generally speaking, we can see that the peatland drainage water had relatively low residence times, especially compared with the streams recharging outside the peatland area. Some previous studies have indicated peatland pore water mean residence times of less than one year for the uppermost 100 cm [73,74], which was confirmed also in the case of the Šijec bog. Two drainage stream samples (W1 and W2) indicated residence times of 61 and 45 days, respectively, while the drainage stream sample W3 indicated a residence time of approximately 5 months. It can be assumed that stream W3 represented a drainage of different dynamics than streams W1 and W2. Due to the later establishment of the pore water sampling points, we started the measurements of such in August 2021, and only performed several measurements of the pore water in October 2021 and June 2022. The seasonal variation and amplitude in the pore water isotopic signatures through the hydrologic year could not be confirmed, since we only had water samples available with high isotopic values. But the tendency of the analyzed samples correlated well with the seasonal variability at other sample sites.

A conservative estimate of the pore water residence time was made based on the correlation between the streams' (N1, N2, W1, W2, and W3) average ^{18}O value for the sampling dates 1/8/2021 and 1/9/2021 (for these dates, pore water samples are also available) with their estimated residence times. A good correlation was observed (r = 0.99). In both cases, the pore water residence time was less than one year (Table 3). The percolation to depth in P1 was estimated at 185 days, while in P2, it was 208 days. The residence time in P2 was already high at a depth of 30 cm, which was most likely due to the groundwater inflow, which can also be supported by an increase in the Ca and Mg content. The increase in the residence time at depths from 60 to 90 cm was significantly smaller than the increase at 30 cm to 60 cm. This was supported by the results of McDonald et al., 2023 [74], who found that below depths of 1 m, the isotope concentrations of the pore water were no longer distinguishable from the long-term precipitation average, due to the mixing with older water.

Table 3. Residence times in the pore water.

Depth	P1	P2
	Residence Time (Days)	
30	67	185
60	164	208
90	185	208

4.2.2. Physico-Chemical Parameters and Chemical Composition

The average measured pH values for the karst stream were 7.8 and 7.9 at the measuring points N1 and N2, respectively. The streams in the eastern area of the Julian Alps typically had pH values from 7.7 to 8.5 [75]. The electrical conductivity (EC) values ranged from 315 to 480 µS/cm, with higher values recorded at the sampling point N2. The stream was well oxygenated, indicating the Eh (490 mV) and dissolved oxygen values (90–100%) (Table 4) from the stream. The stream therefore represented a typical karst stream and the typical conditions for the surface waters in the vicinity of the Šijec bog on the Pokljuka plateau, with no influence from the peatland.

Table 4. Average values for the physico-chemical parameters measured in all the samples. N—number of measurements; EC—electrical conductivity; Eh—reduction potential; DO—dissolved oxygen.

	N	pH	EC (µS/cm)	Eh (mv)	DO (mg/L)	DO (%)
N1	10	7.8	373.5	487.0	10.2	94.0
N2	10	7.9	406.9	492.6	10.8	99.6
W1	10	7.0	78.1	440.4	9.5	89.7
W2	10	6.4	55.2	439.0	6.6	61.5
W3	10	6.8	147.7	448.1	6.7	84.5
S1	9	4.2	25.9	493.6	8.1	86.8
S2	9	4.1	37.7	500.8	8.5	93.3
S3	9	4.3	27.3	495.4	8.1	89.2
P1-30	4	4.4	79.0	515.3		
P1-60	4	4.4	85.0	517.0		
P1-90	4	4.4	74.7	509.1		
P2-30	4	4.4	46.4	483.5		
P2-60	4	4.6	54.6	482.8		
P2-90	4	5.2	114.5	432.4		

The surface pools had a low pH, ranging from 3.4 to 4.6, and a low EC, with values from 17 to 53 µS/cm (Table 4). The streams on the edge of the peatland exhibited the effect of mixing the karst stream water with the peatland drainage. At the W2 measuring point closest to the peatland (Figure 1), the average pH and EC values were 6.4 and 55.2 µS/cm, respectively. Both values increased downstream as the distance from the peatland increased (sampling point W1, average pH value 7, and average EC value 78 µS/cm). The sampling point W3 represented the farthest location that was still under the influence of the peatland drainage and represented the peatland outflow from a SW direction (Figure 1). The average measured pH here was 6.8, while the EC value increased to an average value of 148 µS/cm (Table 4). The redox potential values were high, indicating oxidizing conditions. The streams with peatland drainage had values of approximately 440 mV, while the still waters in the surface pools had values around 500 mV.

The level of dissolved oxygen in the surface pools decreased with depth, which indicated a gradual change to the presumed anoxic conditions. As we took measurements in the upper layers of the pools, the values of dissolved oxygen were high (>85%). The sampling points W1 and W3 along the streams influenced by drainage were both well oxygenated. Point W2, located in the immediate vicinity of the peatland, showed lower

levels of dissolved oxygen (61.5%, Table 4), indicating the influence of the anoxic conditions in the peatland.

The pore water had characteristics similar to those of the surface pools. In both locations (P1 and P2), the water was acidic. In the E part of the peatland (P1), the average pH with a value of 4.4 did not change with depth. In contrast, the average pH value increased with depth in location P2, measuring 4.2 at 30 cm, 4.4 at 60 cm, and 4.9 at 90 cm. A difference in the EC values was also observed among the locations, as the average values for location P1 remained similar with depth (75–85 µS/cm), while in location P2, the values increased from 46 µS/cm (30 cm) to 115 µS/cm (90 cm). The consistent increase in pH and EC with depth at location P2 could be due to an additional water source that influenced the deeper layer of the peat profile, as shown in Lhosmot et al. [16]. The results of the Eh measurements were relatively high and indicated oxidizing conditions in all samples, due to the sampling method. The samples were exposed to the atmosphere for 24 h before collection, which could have impacted the Eh measurements.

Due to the nature of the Macrorhizon method, we were not able to properly measure the levels of dissolved oxygen in the pore water. With multiple measurements taken after the collection of the pore water, we constructed the saturation curve in relation to time (Figure 4). Following a rapid increase in the dissolved oxygen content, the curve gradually flattened and stabilized.

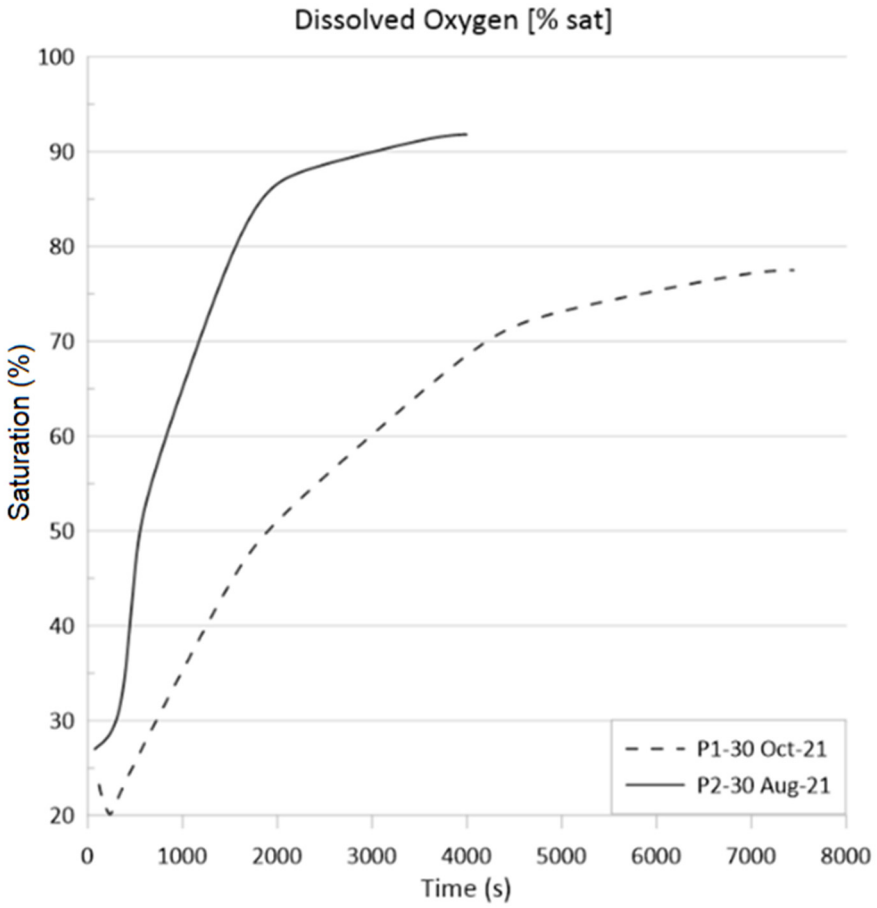

Figure 4. Saturation curves showing two separate measurements of dissolved oxygen in relation to time after the collection.

The chemical composition of the karst streams was similar to that of rivers in the surrounding valleys of the Pokljuka plateau, such as the Triglavska Bistrica River [39]. High concentrations of Ca (Figure 5) and geological maps [43,46] indicated limestone as the predominating lithology surrounding the Šijec bog.

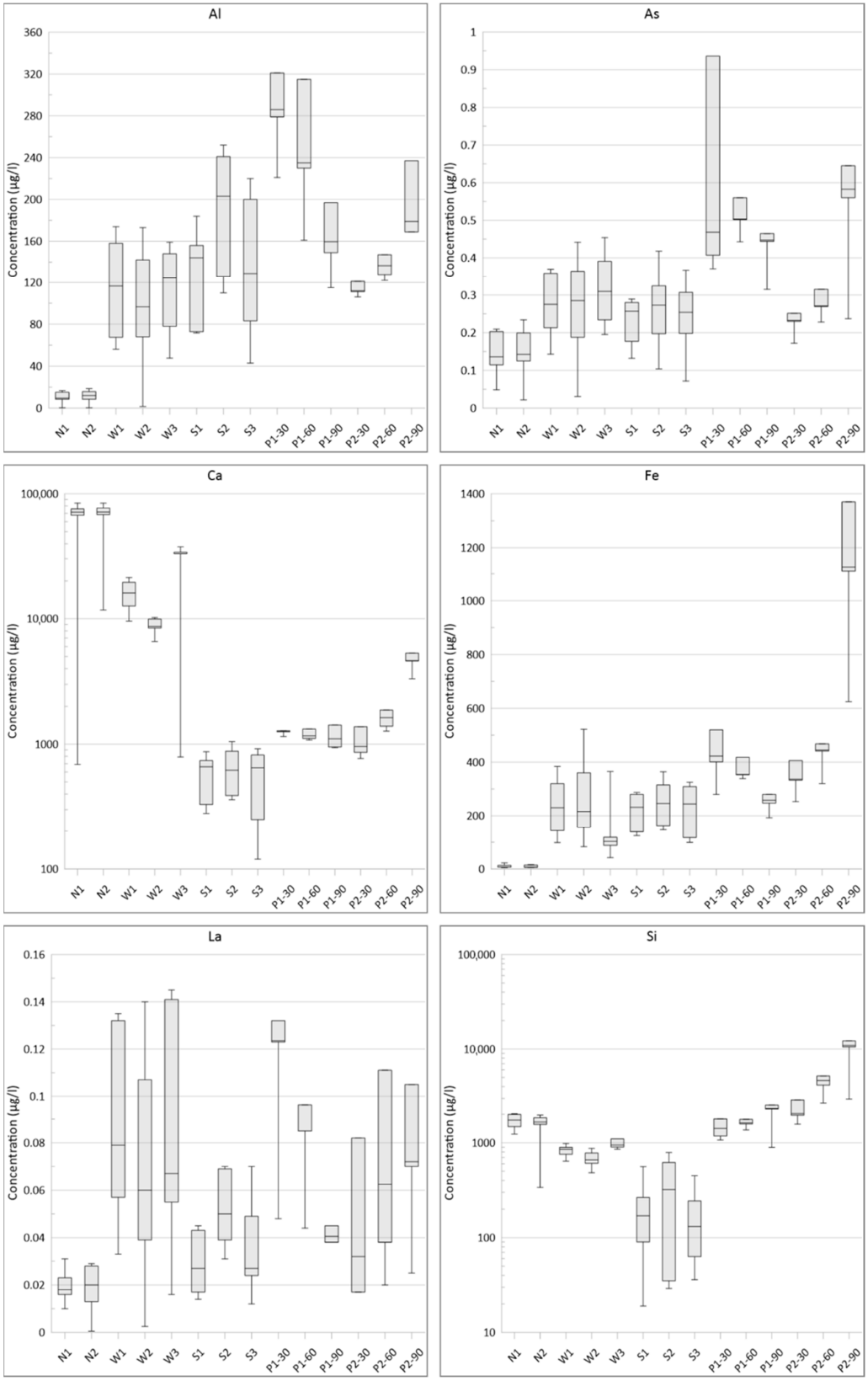

Figure 5. Box plots for elements Al, As, Ca, La, Fe, and Si. The box represents the 25th and 75th percentile, the line represents the median value. The whiskers represent the minimum and maximum. The y-axis for Ca and Si is in the logarithmic scale for better presentation. The sample names are listed on the x-axis, as labelled on Figure 1.

Due to the acidic environment of the surface pools, the particles deposited from the atmosphere, which included elements such as Al, Ba, Ce, Fe, and V, were easily dissolved. In the streams, these particles remained solid. The highest concentrations of these elements were therefore found in the surface pools, and the lowest in the karst streams (Figure 5). In contrast, the opposite was observed for the particles related to the surrounding geology, lithology, and soils (Ca, Mg, Si, and Sr). They had the highest concentrations in the karst streams and the lowest concentrations in the surface pools. The influence of drainage from the peatland was evident in the composition of the stream water, as the concentrations of elements that were more easily dissolved in acidic water (Al, Ba, Ce, Fe, and V) were similar to the concentrations in the surface pools. However, as the drainage mixed with the karst stream water, the contents of those elements originating from the lithology (Ca, Mg, Si, and Sr) were higher compared with those in the surface pools.

The elements that are not easily dissolved, such as As, Co, Cr, Cu, Ni, Rb, and Sb, are present in the surface pools and the drainage in slightly higher concentrations compared with the karst streams, as the acidity of the peatland waters increases their dissolution.

The pore water had a similar chemical composition to the surface pools, although most concentrations were higher in the pore water, due to the binding to the dissolved organic matter (DOM) and the enrichment over time. For most of the elements (Al, As, Ca, Ce, Co, Cr, Cu, Fe, La, Mo, Nd, Y, and Zr) the trends were reversed at sites P1 and P2. Fe did not exhibit any further changes. Compared with the surface pools, the concentration in the pore water increased, but then slowly decreased with depth (location P1). The redox reaction seemed to affect the elements close to the surface, while deeper, the conditions stabilized. The concentrations decreased with depth in location P1 and increased with depth in location P2. This further emphasized the differences between the locations. As previously mentioned, a sudden increase in Ca concentration between the depths of 60 and 90 cm (1598 μg/L and 4470 μg/L, respectively) indicated the possibility of an additional water source in the peat depression below site P2.

4.3. Cluster Analysis of Chemical Composition and Seasonal Variability

We performed a cluster analysis (using Ward's method and Euclidean distances) to group all the samples based on their chemical composition, to observe the possible differences between them. The cluster analysis resulted in six clusters (Figure 6). Majorly, it separated them by water type (karst stream, drainage, surface pools, and pore water). Additionally, it separated the drainage based on the location. One cluster contained samples from locations W1 and W2, while the other cluster included samples from location W3, with one sample from the karst stream. This could be attributed to the distance of the location W3 from the peatland and its similarities to the karst stream properties (pH, chemical composition). Location W3 exhibited a closer relationship with the karst stream locations in the cluster analysis results compared with the other drainage streams. The fourth group included samples taken from the surface pools. The last two clusters were represented mainly by the pore water, with one group including more P1 samples, and the other including more P2 samples. Both groups also included few surface pool samples.

A statistical ANOVA analysis was performed to observe the relationships between the water types, the locations of sampling, and the seasons. Due to the distinct difference between the water types, we performed a second cluster analysis (Ward's method and 1-Pearson r) using the geochemical data on each individual group (Figure 7). Even though the W3 samples formed a separate group, we included them with the other drainage stream samples, as the differences were only observed in the elements related to lithology and soils. Additionally, P2-90 formed an individual group, but due to the low numbers of samples, we included them with the other P2 and pore water samples. For an easier interpretation of the individual clusters, they were named based on their similarities and not according to their position on the tree diagram.

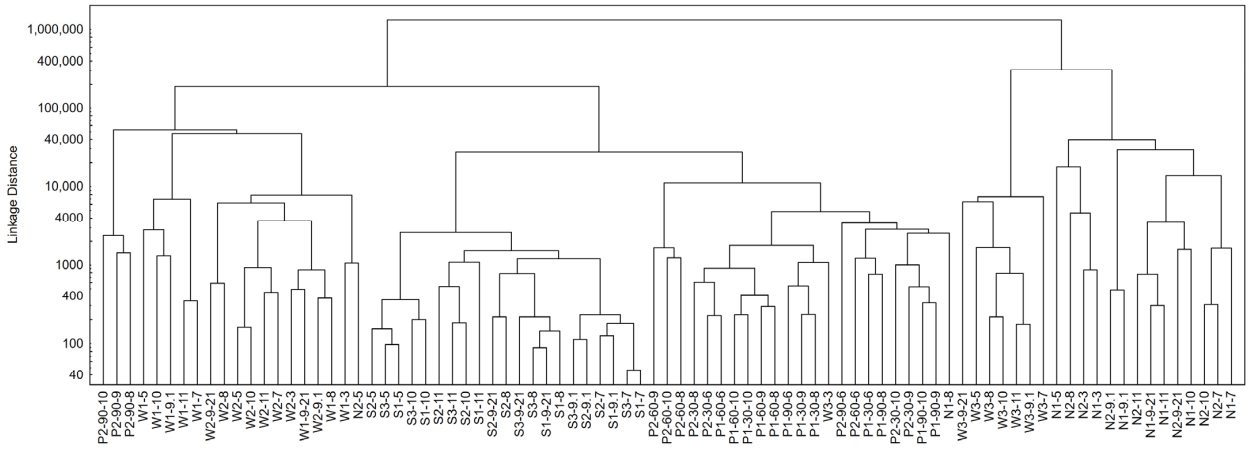

Figure 6. Cluster analysis of all the water samples.

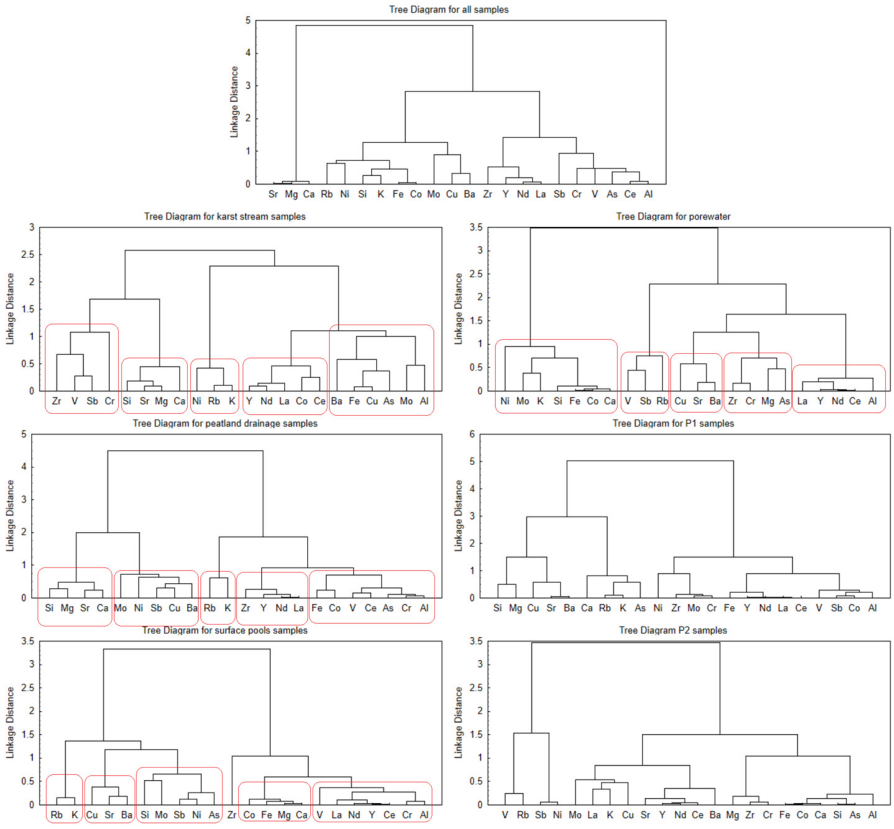

Figure 7. Cluster analysis results for each separate water type. Cluster groups are marked for the main water types (karst stream, drainage stream, surface pool, and pore water). The figure also includes a cluster analysis of all the samples and the individual locations of the pore water. Included in the analysis are measured elemental concentrations.

The elements in the karst stream included in cluster 1 (Ca, Mg, Si, Sr) largely originated from the dissolution of the carbonate lithology in the bedrock of the karstic stream. A similar trend was observed in Serianz et al. [76]. The concentrations showed a slight seasonal variation (Figure 8), with higher values in the late summer and fall, coinciding with the higher temperatures and the rainfall season. Lower values were observed in the winter and spring, when the dissolution rates could be affected by low temperatures. The cluster included elements commonly found in carbonates (Ca, Mg, Sr). The elements in cluster 2 and 3 (Al, As, Ba, Cu, Fe, Mo and Ce, Co, La, Nd, Y) mainly represented the atmospheric deposition of predominantly geogenic origin. They both had peaks in the late summer and

autumn seasons; however, the autumn 2021 peak was more pronounced in cluster 2. Also, the karst stream in October 2020 was partially frozen, causing the elements in both clusters to show a drop in their concentrations (Figure 8). The frozen conditions created a barrier and affected the gaseous exchange between the air and water [77]; therefore, affecting the atmospheric deposition and slowing the dissolution rate. The increase was observed after the ice melted. Although the decrease in the elements was also observed in cluster 3, the increase was not as pronounced. While the average level of PM10 particles was similar in the years 2020 and 2021 [78,79], there was an increase in the particle content in winter 2020 (pre-pandemic) and in summer and autumn 2021 [50]. The larger 2021 peak of the cluster 2 elements could therefore also be due to the increase in tourism and traffic on the Pokljuka plateau after the COVID season, which indicates the elements could be of anthropogenic origin or impacted by anthropogenic activities (resuspension of road dust). Consequently, all these elements mainly originated from the atmospheric deposition. Cluster 4 represented the elements of mostly anthropogenic origin (Cr, Sb, V, Zr). Cluster 5 (K, Ni Rb) had peaks in the winter and was predominately geogenic in origin. A statistical ANOVA analysis showed that in the karst stream elements, Al, As, K, Mg, Sb, Si, and Sr were sensitive to seasonal changes. They had lower values in the spring and winter with the exception of K, which had the highest values in the winter. Mg, Si, and Sr showed a larger variability in the spring compared with the other seasons. The locations of the sampling of the karst streams were similar.

Cluster 1 (Ca, Mg, Si, Sr) in streams with peatland drainage represented the influence of carbonates, which originated from the stream bedrock and the surrounding lithology. Although clusters 2–4 were similar to the ones in the karst stream, they varied slightly. The elements appeared in higher concentrations compared with the karst stream and had smaller or similar concentration values compared with the surface pools. It mostly included metals and REE. The three clusters were under the influence of the peatland drainage, while still retaining similar properties to the karst stream. Cluster 4 was represented by Ba, Cu, Mo, Ni, and Sb, which had a different seasonal variability with particularly increased concentrations in 2021, especially in the late summer 2021. Cluster 5 (K, Rb) indicated a different seasonal behavior, with higher concentrations in the winter. The elements with statistical differences during the seasons in the peatland drainage water were Al, As, Ce, Cr, Fe, La, Nd, Ni, and V. All showed a similar pattern with higher concentrations in the summer and autumn and lower in the winter and spring. Between the sampling locations, the differences showed in the concentrations of Ca, Mg, Sb, Si, and Sr, due to the W3 sampling point with more similarities with the karst stream.

In the surface pools, most elements were present in low concentrations (Figure 5), which was also evident from the low electrical conductivity values (average 30.3 µS/cm). The pH in the surface pool water was 4, indicating a highly acidic environment. Most of the atmospheric deposition was quickly dissolved and bound to organic matter, as also observed by [17]. Cluster 1 (Ca, Mg, Fe, Co) and cluster 2 (Al, Ce, Cr, La, Nd, Y, V) comprised elements that were readily soluble in this environment. The elements in cluster 2 were more affected by the autumn 2021 compared with cluster 1. Cluster 3 (Ba, Cu, Sr) showed an increase in the concentration of the elements in the late summer 2021 and spring 2022. This could be due to the increased influence of anthropogenic sources after COVID. Zupančič & Bozau [70] confirmed the variations in the concentrations of elements in Sphagnum moss, including in the Šijec bog on the Pokljuka plateau. Cluster 4 included elements that were less soluble in the acid environment (As, Mo, Ni, Sb, Si). Similar to the previous water types, cluster 5 exhibited different seasonal variability of K and Rb with the highest concentrations in the winter and the lowest in the autumn. In the surface pools, most elements showed statistical differences in the concentrations between seasons. This occurred because during the winter, the pools were covered with snow or were frozen, which impacted the rate of dissolution. In the spring, the concentrations were still lower compared with the summer and autumn, but higher compared with the winter. The locations of sampling did not show differences between each other.

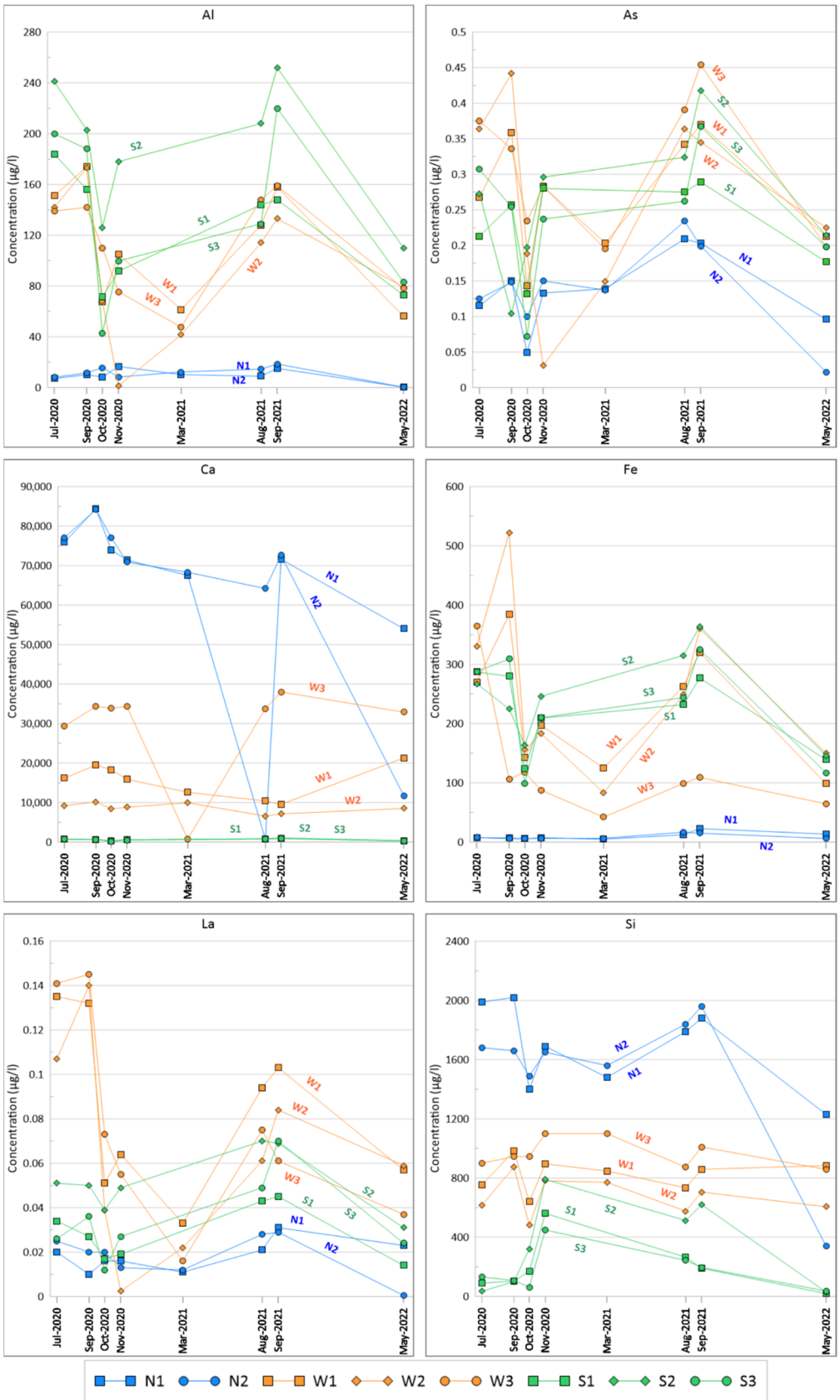

Figure 8. Seasonal changes as shown in the concentration levels of Al, As, Ca, Fe, La, and Si in the different water types.

The concentrations of the components in the pore water from each location were similar, although slight variations were observed. A statistical cluster analysis for all the pore water samples distinguished five clusters. Clusters 1 and 2 represented the elements with well-defined differences in depth and trends between locations (Ca, Co, Fe, K, Mo, Ni, Si and Al, Ce, La, Nd, Y). These elements were found in their highest concentrations at a depth of 30 cm in location P1, while the lowest values were attributed to the location P2 at a depth of 30 cm. The elements included in Cluster 1 followed this trend; however, the concentrations between the locations had less variation. The exception was location P2 at a depth of 90 cm, where far higher values were observed, at three times higher compared with a depth of 60 cm at the same location. Cluster 3 (Ba, Cu, Sr) was influenced by changes throughout the year, with lower concentrations in the spring compared with the autumn. The variations throughout the year for the elements in terms of other clusters were small. The elements from Cluster 3, as well as Cluster 4 (As, Cr, Mg, Zr) did not show the previously described trends (e.g., Mg in cluster 4 departed from the trend in June 2022, where in location P1 the concentration increased with depth, while in location P2 it decreased with depth). Cluster 5 included the elements Rb, Sb, and V, which all had similar trends in both locations (P1 and P2). The pore water generally showed stable concentrations throughout the year, with smaller variations for the elements Ba, Rb, Sr, and V. However, the sampling location and depth showed large differences in most elements, indicating that it was important to consider the locations separately.

To compare the pore water between the locations, a statistical *t*-test was also performed. It showed good correlates between the locations for the elements Ba, Cr, Cu K, La, Mo, Ni, Rb, Sb, Sr, V, and Zr), while the elements Al, As, Ca, Ce, Co, Fe, Mg, Nd, Si, and Y were not comparable between the locations, which additionally strengthened the possibility of an additional water source with the elements with a predominately geogenic origin. Due to the differences between the pore water sampling locations, a cluster analysis was performed for the individual locations. The low number of sampling campaigns throughout the year also influenced the detection of possible seasonal variations. However, cluster 5 for location P1 indicated the possible influence of the seasons, as it included elements that were associated with high values in the winter (particularly K and Rb). More samples across the different seasons would be required to better understand the variations and influences in the pore water.

Statistically comparing the seasons based on the water types, the differences were especially apparent in the summer and autumn, due to the higher temperatures in the summer and the rainfall season in the autumn. It mostly showed as lower element concentrations in the karst stream, where the water temperature was lower compared with the surface pools and the edge of the peatland (approximately 8.5 °C in the karst stream and over 25 °C in the surface pools). In the winter and spring, the differences were visible; however, they were not as pronounced as in the summer and autumn and were mostly observed in metals.

Most of the elements (Al, As, Ca, Ce, Co, Cu, Fe, La, Mg, Nd, Ni, Rb, Sr, V, and Y) showed the largest variation between the water types, with many of them (Al, As, Ce, Co, Fe, Mg, Si, and Sr) also showing variations between the sampling locations of the same water type. The elements Ba, Ca, Cr, Cu, La, Mg, Nd, Rb, Sb, Sr, V, Y, and Zr were influenced by the seasons. However, the elements Ba, Cr, Cu, K, La, Mo, Nd, Ni, Rb, Sb, V, Y, and Zr also showed a large percentage of unexplained variance, indicating more reasons for their variations. Most of these were most likely also dependent on the anthropogenic influence.

4.4. Relationship between Pore Water, Surface Pools, and Drainage

Although the pore water and surface pools had similar chemical compositions, most elements appeared in higher concentrations in the pore water, especially in the upper layers (30 cm) at location P1 and in the lower layers (90 cm) at location P2. This difference further suggested differences in the development stage of the peatland. While the E part of the peatland was in an ombrotrophic peat phase, which was implied from its slight dome

shape and stable pH with depth, the NW part could be determined as minerotrophic peat. The difference in their natures was already presumed from the shape of the peat basin, as studied in Pezdir et al. [37]. An additional source of water (groundwater or surface runoff water from the surrounding karst area) could explain the increase with depth in the concentrations of the components, pH values, and electrical conductivity values.

In terms of the chemical compositions, streams with drainage from the peatland were similar to the karst stream and both exhibited calcium types (Figure 9). However, they were enriched in some elements (Al, As, Co, Fe, V, Y, Zr, and REE) due to the influence of the peatland. The concentrations of the elements originating from the surrounding lithology and soil (Ca, K, Mg, Si, and Sr) were lower than in a typical karst stream. Some elements, especially antimony, showed a high affinity for binding to organic matter [80] and were not readily removed from the peatland, as was also evident from the similar concentrations in both types of streams, while the concentrations in the surface pools were higher and decreased with depth in the pore water.

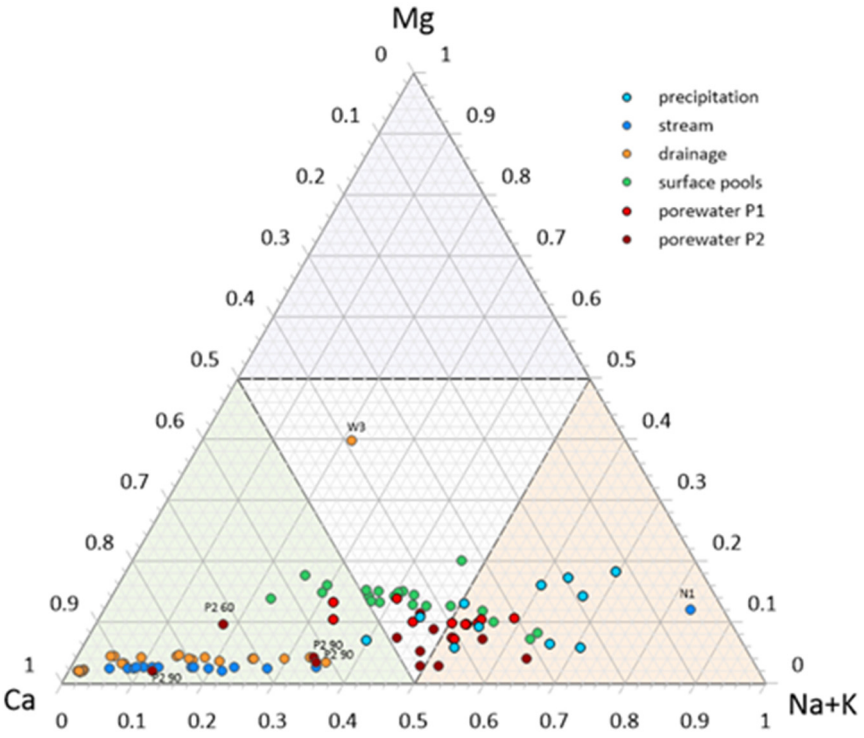

Figure 9. Ternary diagram showing the chemical composition of all the water samples. The outliers are marked with labels.

Precipitation has a higher concentration of potassium and sodium in relation to calcium and magnesium. The chemical composition of the surface pools, as well as the pore water, has an affinity for both the calcium and sodium types, emphasizing the importance of precipitation as a water source for the peatland. However, most samples did not have any dominant types (Figure 9). The low Ca concentration of the N1 sample could be the result of a sampling or analytical error, while the high MG concentrations of the W3 sample in March 2021 could be due to the winter conditions and the location of the W3 sampling point. The high Ca concentrations of the lower layers in pore water P2 are emphasized.

The chemical composition reflects the two different drainage systems in the NW (sampling locations W1 and W2) and the SW (location W3). However, location W3 was furthest from the peatland, which could have influenced the composition of the water. Also, the fact that there was no pore water sampling location in the SW part of the peatland needs to be taken in account, and therefore, we cannot determine whether the differences were related to variations in the chemical composition of the pore water within the peatland.

The ternary diagram also emphasizes the differences between the pore water sampling locations, as well as the different chemical composition at 90 cm at location P2 (Figure 9). While most pore water had either no affinity or sodium type, the pore water at 90 cm had a calcium affinity.

5. Conclusions

The results of the chemical composition of the pore water and the isotope analysis highlight the variations within the area of the peatland, potentially indicating a heterogeneous hydrological structure. In the NW area of the peatland, there appeared to be an additional groundwater source, which was recharging the examined section. This was evident as an increase in the Ca and Mg content, as well as in the isotopic signature. The origin of the source could be a groundwater spring or surface runoff from a surrounding slope. This further proves that the northwestern part is not composed of ombrotrophic peat but rather of minerotrophic peat. However, the E part of the peatland showed a more stable chemical elemental composition that gradually decreased with depth. This decrease was due to the age of the peat and the lower concentrations of mineral matter in the peat, which was based on the results of the radiocarbon dating [81]. Seasonal patterns in the water isotopic (^{18}O and ^{2}H) signatures could be observed, which corresponded to the variability in precipitation. Moreover, it was also estimated that the residence times of the drainage streams and the pore water were less than one year.

In order to evaluate the relationship between the peat, the degradation of the organic matter, and water, we must further consider the composition of the peat mineral matter. We observed the chemical and isotopic composition of precipitation as the water source, streams that were not connected to the peatland as the background values, streams that were connected to the drainage from the peatland, surface pools on the peatland, and the pore water. As the surface pools represented the contact between the peatland water and the atmosphere, there was a very small amount of dissolved mineral matter. As seen in the pore water, the concentration of the dissolved elements increased, which was mainly attributed to the acidic and anoxic peatland environment. Some major and trace elements were partially removed from the peatland (e.g., La, and Ni), while others were retained or moved within the peat profile (e.g., Cu). The increase in the mobile elements was observed in the streams that drained the peatland. The chemical composition of the streams with drainage showed the increase in the concentration of the elements that were preferentially dissolved (Al, Ba, Ce, Fe, V, and REE). Additionally, the concentration of the elements that were not easily dissolved (As, Co, Cr, Cu, Ni, Rb, and Sb) were more comparable to the surface pools than the background values. Due to the high concentrations of Ca, Mg, Si, and Sr in a karst stream, their concentration in the drainage could not be properly assessed. However, comparing the elemental concentrations in the surface pools and the drainage, we observed that they were higher in the surface pools for many elements. Therefore, as the elements were not completely removed from the peatland, their analyzed concentrations in peat did not directly reflect the atmospheric deposition. Variations in the pore water throughout the peatland, together with the water balance, need to be further studied. For a better understanding of the NW area of the peatland, additional hydrogeological studies must be performed in the area.

We present the processes that occur and change in the water composition in peatlands. Peatlands are commonly exploited and altered for energy production and agricultural purposes. Additionally, peatlands present an important part of the terrestrial carbon cycle, which makes them important for consideration in terms of climate change. While this study focused on the effects of peatland on water chemical composition that occur naturally, in altered peatlands, these effects are much more important and can greatly influence or change the environment in the long-term period. Therefore, peatland hydrology is an important aspect to carefully consider, especially in areas where the peatlands cover large surface areas.

Author Contributions: Conceptualization, V.P. and M.G.; Methodology, V.P. and L.S.; Software, V.P. and L.S.; Validation, V.P., L.S., and M.G.; Formal Analysis, V.P.; Investigation, V.P. and L.S.; Resources, M.G.; Data Curation, V.P. and L.S.; Writing—Original Draft Preparation, V.P.; Writing—Review and Editing, V.P., L.S., and M.G.; Visualization, V.P.; Supervision, M.G.; Project Administration, M.G.; Funding Acquisition, M.G. All authors have read and agreed to the published version of the manuscript.

Funding: The presented study was funded by the Slovenian Research and Innovation Agency (ARIS) in the frame of the young researcher program and in the frame of the research program, Groundwater and Geochemistry (P1-0020). Financial assistance was also provided by the "Slovenian National Commission for UNESCO, National Committee of the International Geoscience and Geoparks Programme".

Institutional Review Board Statement: Not applicable.

Informed Consent Statement: Not applicable.

Data Availability Statement: The data presented in this study are available on request from the corresponding author.

Acknowledgments: We thank the reviewers for their constructive comments, which helped to improve the paper.

Conflicts of Interest: The authors declare no conflicts of interest.

References

1. Assiri, M.; Sartori, A.; Vignoli, G.; Massironi, M.; Silvestri, S. Characterizing Alpine peatlands from drones: A case study. In Proceedings of the EGU General Assembly 2022, Vienna, Austria, 23–27 May 2022. [CrossRef]
2. Heijmans, M.M.; Mauquoy, D.; van Geel, B.; Berendse, F. Long-term effects of climate change on vegetation and carbon dynamics in peat bogs. *J. Veg. Sci.* **2008**, *19*, 307–320. [CrossRef]
3. Fracasso, I.; Dinella, A.; Giammarchi, F.; Marinchel, N.; Kołaczek, P.; Lamentowicz, M.; Marcisz, K.; Łokas, E.; Miecznik, M.; Bragazza, L.; et al. Climate and human impacts inferred from a 1500-year multi-proxy record of an alpine peatland in the South-Eastern Alps. *Ecol. Indic.* **2022**, *145*, 109737. [CrossRef]
4. Holden, J. Peatland hydrology. In *Peatlands: Evolution and Records of Environmental and Climate Changes*; Martini, I., Cortizas, A.M., Chesworth, W., Eds.; Elsevier B.V.: Oxford, UK, 2006; pp. 319–346.
5. Holden, J.; Chapman, P.J.; Labadz, J.C. Artificial drainage of peatlands: Hydrological and hydrochemical process and wetland restoration. *Prog. Chem. Org. Nat. Prod. Phys. Geogr.* **2004**, *28*, 95–123. [CrossRef]
6. Wilson, L.; Wilson, J.; Holden, J.; Johnstone, I.; Armstrong, A.; Morris, M. Ditch blocking, water chemistry and organic carbon flux: Evidence that blanket bog restoration reduces erosion and fluvial carbon loss. *Sci. Total Environ.* **2011**, *409*, 2010–2018. [CrossRef] [PubMed]
7. Li, Z.; Gao, P.; Lu, H. Dynamic changes of groundwater storage and flows in a disturbed alpine peatland under variable climatic conditions. *J. Hydrol.* **2019**, *575*, 557–568. [CrossRef]
8. Holden, J.; Shotbolt, L.; Bonn, A.; Burt, T.P.; Chapman, P.J.; Dougill, A.J.; Fraser, E.D.G.; Hubacek, K.; Irvine, B.; Kirkby, M.J.; et al. Environmental change in moorland landscapes. *Earth Sci. Rev.* **2007**, *82*, 75–100. [CrossRef]
9. Ramchunder, S.J.; Brown, L.E.; Holden, J. Environmental effects of drainage, drain-blocking and prescribed vegetation burning in UK upland peatlands. *Prog. Chem. Org. Nat. Prod. Phys. Geogr.* **2009**, *33*, 49–79. [CrossRef]
10. Clymo, R.S. The ecology of peatlands. *Sci. Prog.* **1987**, *71*, 593–614.
11. Biester, H.; Knorr, K.H.; Schellekens, J.; Basler, A.; Hermanns, Y.M. Comparison of different methods to determine the degree of peat decomposition in peat bogs. *Biogeosciences* **2014**, *11*, 2691–2707. [CrossRef]
12. Charman, D. *Peatlands and Environmental Change*; John Wiley & Sons Inc.: Hoboken, NJ, USA, 2002.
13. Chesworth, W.; Martínez Cortizas, A.; García-Rodeja, E. The redox-pH approach to the geochemistry of the Earth's land surface, with application to peatlands. In *Peatlands: Evolution and Records of Environmental and Climate Changes*; Martini, I., Cortizas, A.M., Chesworth, W., Eds.; Elsevier B.V.: Oxford, UK, 2006; pp. 175–195. [CrossRef]
14. Hansson, S.V.; Tolu, J.; Bindler, R. Downwash of atmospherically deposited trace metals in peat and the influence of rainfall intensity: An experimental test. *Sci. Total Environ.* **2015**, *506–507*, 95–101. [CrossRef]
15. Lhosmot, A.; Collin, L.; Magnon, G.; Steinmann, M.; Bertrand, C.; Stefani, V.; Toussaint, M.-L.; Bertrand, G. Restoration and meteorological variability highlight nested water supplies in middle altitude/latitude peatlands: Towards a hydrological conceptual model of the Frasne peatland, Jura Mountains, France. *Ecohydrology* **2021**, *14*, e2315. [CrossRef]
16. Lhosmot, A.; Steinmann, M.; Binet, P.; Gandois, L.; Moquet, J.-S.; Stefani, V.; Toussaint, M.-L.; Boetsch, A.; Loup, C.; Essert, V.; et al. Origin and fate of dissolved inorganic carbon in a karst groundwater fed peatland using δ13CDIC. *Chem. Geol.* **2023**, *616*, 121254. [CrossRef]

17. Biester, H.; Hemanns, Y.-M.; Martinez Cortizas, A. The influence of organic matter decay on the distribution of major and trace elements in ombrotrophic mires—A case study from the Harz Mountains. *Geochim. Cosmochim. Acta* **2012**, *84*, 126–136. [CrossRef]
18. Pokrovsky, O.S.; Schott, J.; Dupré, B. Trace element fractionation and transport in boreal rivers and soil porewaters of permafrost-dominated basaltic terrain in Central Siberia. *Geochim. Cosmochim. Acta* **2006**, *70*, 3239–3260. [CrossRef]
19. Aiken, G.R.; Hsu-Kim, H.; Ryan, J.N. Influence of Dissolved Organic Matter on the Environmental Fate of Metals, Nanoparticles, and Colloids. *Environ. Sci. Technol.* **2011**, *45*, 3196–3201. [CrossRef] [PubMed]
20. Broder, T.; Biester, H. Linking major and trace element concentrations in a headwater stream to DOC release and hydrologic conditions in a bog and peaty riparian zone. *Appl. Geochem.* **2017**, *87*, 188–201. [CrossRef]
21. Holden, J.; Burt, T.P. Runoff production in blanket peat covered catchments. *Water Resour. Res.* **2003**, *39*, SWC61–SWC69. [CrossRef]
22. Hayashi, M.; Quinton, W.L.; Pietroniro, A.; Gibson, J.J. Hydrologic functions of wetlands in a discontinuous permafrost basin indicated by isotopic and chemical signatures. *J. Hydrol.* **2004**, *296*, 81–97. [CrossRef]
23. Ala-aho, P.; Soulsby, C.; Pokrovsky, O.S.; Kirpotin, S.N.; Karlsson, J.; Serikova, S.; Vorobyev, S.N.; Manasypov, R.M.; Loiko, S.; Tetzlaff, D. Using stable isotopes to assess surface water source dynamics and hydrological connectivity in a high-latitude wetland and permafrost influenced landscape. *J. Hydrol.* **2018**, *556*, 279–293. [CrossRef]
24. Dansgaard, W. Stable isotopes in precipitation. *Tellus* **1964**, *16*, 436–468. [CrossRef]
25. Gat, J.R.; Gonfiantini, R. *Stable Isotope Hydrology Deuterium and Oxygen-18 in the Water Cycle*; International Atomic Energy Agency (IAEA): Vienna, Austria, 1981.
26. Rozanski, K.; Araguás-Araguás, L.; Gonfiantini, R. Isotopic patterns in Global Precipitation. *J. Geophys. Res.* **1992**, *78*, 1–36. [CrossRef]
27. Rodgers, P.; Soulsby, C.; Waldron, S.; Tetzlaff, D. Using stable isotope tracers to assess hydrological flow paths, residence times and landscape influences in a nested mesoscale catchment. *Hydrol. Earth Syst. Sci.* **2005**, *9*, 139–155. [CrossRef]
28. Clark, I.D.; Fritz, P. *Environmental Isotopes in Hydrogeology*; CRC Press: Boca Raton, FL, USA; Taylor & Francis Group: New York, NY, USA, 1997.
29. Glynn, P.D.; Plummer, L.N. Geochemistry and the Understanding of Groundwater Systems. *Hydrogeol. J.* **2005**, *13*, 263–287. [CrossRef]
30. Xu, X.; Zhang, Q.; Tan, Z.; Li, Y.; Wang, X. Effects of water-table depth and soil moisture on plant biomass, diversity, and distribution at a seasonally flooded wetland of Poyang Lake, China. *Chin. Geogr. Sci.* **2015**, *25*, 739–756. [CrossRef]
31. Zhang, L.; Yin, J.; Jiang, Y.; Wang, H. Relationship between the hydrological conditions and the distribution of vegetation communities within the Poyang Lake National Nature Reserve, China. *Ecol. Inform.* **2012**, *11*, 65–75. [CrossRef]
32. van Breemen, N. How Sphagnum bogs down other plants. *Trends Ecol. Evol.* **1995**, *10*, 270–275. [CrossRef] [PubMed]
33. Granath, G.; Strengbom, J.; Rydin, H. Rapid ecosystem shifts in peatlands: Linking plant physiology and succession. *Ecology* **2010**, *91*, 3047–3056. [CrossRef] [PubMed]
34. Tuittila, E.-S.; Juutinen, S.; Frolking, S.; Väliranta, M.; Laine, A.M.; Miettinen, A.; Seväkivi, M.-L.; Quillet, A.; Merilä, P. Wetland chronosequence as a model of peatland development: Vegetation succession, peat and carbon accumulation. *Holocene* **2013**, *23*, 25–35. [CrossRef]
35. Vidic, N.J.; Prus, T.; Grčman, H.; Zupan, M.; Lisec, A.; Kralj, T.; Vrščaj, B.; Rupreht, J.; Šporar, M.; Suhadolc, R.; et al. *Tla Slovenije s Pedološko Karto v Merilu 1:250 000 = Soils of Slovenia with Soil Map 1:250 000*; Evropska Komisija, Skupni Raziskovalni Center (JRC)/European Commission Joint Research Centre (JRC)/Publication Office of the European Union: Luxembourg, 2015; p. 152. [CrossRef]
36. Tanneberger, F.; Tegetmeyer, C.; Busse, S.; Barthelmes, A.; Shumka, S.; Moles Mariné, A.; Jenderedjian, K.; Steiner, G.M.; Essl, F.; Etzold, J.; et al. The peatland map of Europe. *Mires Peat* **2017**, *19*, 1–17. [CrossRef]
37. Pezdir, V.; Čeru, T.; Horn, B.; Gosar, M. Investigating peatland stratigraphy and development of the Šijec bog (Slovenia) using near-surface geophysical methods. *Catena* **2021**, *206*, 105484. [CrossRef]
38. Gale, L.; Kukoč, D.; Rožič, B.; Vidervol, A. Sedimentological and paleontological analysis of the Lower Jurassic part of the Zatrnik Formation on the Pokljuka plateau, Slovenia. *Geologija* **2021**, *64*, 173–188. [CrossRef]
39. Serianz, L.; Cerar, S.; Vreča, P. Using stable isotopes and major ions to identify recharge characteristics of the Alpine groundwater-flow dominated Triglavska Bistrica River. *Geologija* **2021**, *64*, 205–220. [CrossRef]
40. Comas, X.; Slater, L.; Reeve, A. Stratigraphic controls on pool formation in a domed bog inferred from ground penetrating radar (GPR). *J. Hydrol.* **2005**, *315*, 40–51. [CrossRef]
41. Andrič, M.; Martinčič, A.; Štular, B.; Petek, F.; Goslar, T. Land-use changes in the Alps (Slovenia) in the fifteenth, nineteenth and twentieth centuries AD: A comparative study of the pollen record and historical data. *Holocene* **2010**, *20*, 1023–1037. [CrossRef]
42. Buser, S. *Osnovna Geološka Karta 1:100,000, Tolmač lista Celovec, L 33-53*; Zvezni Geološki Zavod: Beograd, Serbia, 1975.
43. Jurkovšek, B. *Osnovna Geološka Karta SFRJ—List Beljak in Ponteba, Merilo 1:100,000*; Zvezni Geološki Zavod: Beograd, Serbia, 1987.
44. Šifrer, M. Obseg zadnje poledenitve na Pokljuki. *Geogr. Vestn.* **1952**, *24*, 95–114.
45. Jurkovšek, B. *Osnovna Geološka Karta 1:100,000, Tolmač Listov Beljak in Ponteba, L 33-51, L 33-52*; Geološki Zavod Ljubljana, Zvezni Geološki Zavod: Beograd, Serbia, 1987.
46. Buser, S.; Cajhen, J. *Osnovna Geološka Karta SFRJ—List Celovec, Merilo 1:100,000*; Zvezni Geološki Zavod: Beograd, Serbia, 1978.
47. Buser, S. *Osnovna Geološka Karta SFRJ—List Tolmin in Videm, Merilo 1:100,000*; Zvezni Geološki Zavod: Beograd, Serbia, 1987.

48. Budnar-Tregubov, A. Palinološko raziskovanje barij na Pokljuki in Pohorju. *Geologija* **1958**, *4*, 192–220.
49. Eijkelkamp. *Rhizon Soil Moisture Samplers. Manual*; Royal Eijkelkamp: Giesbeek, The Netherlands, 2022; p. 9.
50. Pezdir, V.; Gaberšek, M.; Gosar, M. Characterization of Atmospheric Deposition as the Only Mineral Matter Input to Ombrotrophic Bog. *Minerals* **2022**, *12*, 982. [CrossRef]
51. Picarro. Picarro L2130-i Isotopic Water Analyzer. 2011. Available online: http://www.ebd.csic.es/lie/PDF/Picarro_L2130-i_Isotopic_Water_Analyzer.pdf (accessed on 2 March 2022).
52. Picarro. *Operation, Maintenance and Troubleshooting L2140-i, L2130-i or L2120-i Analyzer and Peripherals—User's Manual*; Picarro: Santa Clara, CA, USA, 2015; p. 2.
53. IAEA. *WICO 2020 δ18O/δ2H Intercomparison Test Laboratory Report*; IAEA: Vienna, Austria, 2020; p. 8.
54. USGS. *Report of Stable Isotopic Composition Reference Material USGS46 Ice Core Water (Hydrogen and Oxygen Isotopes in Water)*; United State Geological Survey-Reston Stable Isotope Laboratory: Reston, VA, USA, 2019; p. 3.
55. USGS. *Report of Stable Isotopic Composition Reference Material USGS47 Lake Louise Drinking Water (Hydrogen and Oxygen Isotopes in Water)*; United States Geological Survey-Reston Stable Isotope Laboratory: Reston, VA, USA, 2019.
56. USGS. *Report of Stable Isotopic Composition Reference Material USGS48 Puerto Rico Precipitation (Hydrogen and Oxygen Isotopes in Water)*; United States Geological Survey-Reston Stable Isotope Laboratory: Reston, VA, USA, 2020.
57. *Reference Material 8535*; VSMOW Vienna Standard Mean Ocean Water. National Institute of Standards and Technology, U.S. Department of Commerce: Gaithersburg, MD, USA, 2022.
58. Koren, K.; Serianz, L.; Janža, M. Characterizing the Groundwater Flow Regime in a Landslide Recharge Area Using Stable Isotopes: A Case Study of the Urbas Landslide Area in NW Slovenia. *Water* **2022**, *14*, 912. [CrossRef]
59. Craig, H. Isotope variations in meteoric waters. *Science* **1961**, *133*, 1702–1703. [CrossRef]
60. Gat, J.R.; Carmi, I. Evolution of the isotopic composition of atmospheric waters in the Mediterranean Sea area. *J. Geophys. Res.* **1970**, *75*, 3039–3048. [CrossRef]
61. Vreča, P.; Pavšek, A.; Kocman, D. SLONIP—A Slovenian Web-Based Interactive Research Platform on Water Isotopes in Precipitation. *Water* **2022**, *14*, 2127. [CrossRef]
62. Niinikoski, P.I.; Hendriksson, N.M.; Karhu, J.A. Using stable isotopes to resolve transit times and travel routes of river water: A case study from southern Finland. *Isot. Environ. Health Stud.* **2016**, *52*, 380–392. [CrossRef]
63. OriginLab. *OriginPro*; OriginLab Corporation: Northampton, MA, USA, 2019.
64. IJS. SLONIP-Slovenian Network of Isotopes in Precipitation. Available online: https://slonip.ijs.si/accounts/login/?next=/data/6 (accessed on 10 August 2023).
65. *IV-STOCK-1643*; Trace Elements in Eater. National Institute of Standards and Technology, U.S. Department of Commerce: Gaithersburg, MD, USA, 2023.
66. Croghan, C.; Egeghy, P.P. *Methods of Dealing with Values below the Limit of Detection Using SAS*; Southeastern SAS User Group: St. Petersburg, FL, USA, 2003.
67. *Statistica (Data Analysis Software System)*, version 13; TIBCO Software Inc.: Palo Alto, CA, USA, 2017. Available online: http://statistica.io (accessed on 24 March 2024).
68. Berner, E.K.; Berner, R.A. *Global Environment: Water, Air, and Geochemical Cycles*, 2nd ed.; Princeton University Press: Princeton, NJ, USA, 2012; p. 464.
69. Koleša, T. Air Pollution in Februar 2021. *Naše Okolje* **2021**, *28*, 90–99. Available online: https://www.arso.gov.si/o%20agenciji/knji%C5%BEnica/mese%C4%8Dni%20bilten/NASE%20OKOLJE%20-%20Februar%202021.pdf (accessed on 15 February 2023).
70. Zupančič, N.; Bozau, E. Effect of the coronavirus pandemic lockdown to elemental composition of peat mosses. *Environ. Sci. Pollut. Res.* **2022**, *29*, 25473–25485. [CrossRef]
71. Tian, C.; Wang, L.; Kaseke, K.F.; Bird, B.W. Stable isotope compositions (δ2H, δ18O and δ17O) of rainfall and snowfall in the central United States. *Sci. Rep.* **2018**, *8*, 6712. [CrossRef] [PubMed]
72. Vreča, P.; Malenšek, N. Slovenian Network of Isotopes in Precipitation (SLONIP)—A review of activities in the period 1981–2015. *Geologija* **2016**, *59*, 67–83. [CrossRef]
73. Aravena, R.; Warner, B.G. Oxygen-18 composition of Sphagnum, and microenvironmental water relations. *Bryologist* **1992**, *95*, 445–448. [CrossRef]
74. McDonald, R.M.; Moore, P.A.; Helbig, M.; Waddington, J.M. Reduced Net CO_2 Uptake during Dry Summers in a Boreal Shield Peatland. *J. Geophys. Res. Biogeosci.* **2023**, *128/2*, e2022JG006923. [CrossRef]
75. Serianz, L. Hidrogeološka Analiza Iztoka Termalne Vode iz Karbonatnega Vodonosnika Vzhodnega Dela Julijskih Alp. Ph.D. Thesis, Naravoslovnotehniška fakulteta, Univerza v Ljubljani, Ljubljana, Slovenia, 2022.
76. Serianz, L.; Rman, N.; Brenčič, M. Hydrogeochemical Characterization of a Warm Spring System in a Carbonate Mountain Range of the Eastern Julian Alps, Slovenia. *Water* **2020**, *12*, 1427. [CrossRef]
77. Obertegger, U.; Obrador, B.; Flaim, G. Dissolved oxygen dynamics under ice: Three winters of high-frequency data from Lake Tovel, Italy. *Water Resour. Res.* **2017**, *53*, 7234–7246. [CrossRef]
78. Ciglenečki, D.; Gjerek, M.; Kastelic, M.; Koleša, T.; Logar, M.; Matavž, L.; Murovec, M.; Rus, M.; Žabkar, R. *Kakovost Zraka v Sloveniji v Letu 2020*; Ministrstvo za Okolje in Prostor, Agencija Republike Slovenije za okolje: Ljubljana, Slovenia, 2021.
79. Bec, D.; Ciglenečki, D.; Dolšak Lavrič, P.; Gjerek, M.; Koleša, T.; Logar, M.; Matavž, L.; Murovec, M.; Rus, M.; Žabkar, R. *Kakovost Zraka v Sloveniji v Letu 2021*; Ministrstvo za Okolje in Prostor, Agencija Republike Slovenije za Okolje: Ljubljana, Slovenia, 2022.

80. Besold, J.; Eberle, A.; Noël, V.; Kujala, K.; Kumar, N.; Scheinost, A.C.; Pacheco, J.L.; Fendorf, S.; Planer-Friedrich, B. Antimonite Binding to Natural Organic Matter: Spectroscopic Evidence from a Mine Water Impacted Peatland. *Environ. Sci. Technol.* **2019**, *53*, 10792–10802. [CrossRef] [PubMed]
81. Andrič, M.; (ZRC SAZU, Inštitut za arheologijo, Ljubljana, Slovenia). Personal communication, 2019.